IEEE Access
Multidisciplinary | Rapid Review | Open Access Journal

Received July 14, 2019, accepted July 25, 2019, date of publication August 6, 2019, date of current version August 20, 2019.

Digital Object Identifier 10.1109/ACCESS.2019.2933494

Implementation and Analysis of 3D Channel Emulation Method in Multi-Probe Anechoic Chamber Setups

WEIMIN WANG, RURU WANG, HUAQIANG GAO, AND YONGLE WU

Beijing Key Laboratory of Work Safety Intelligent Monitoring, School of Electronic Engineering, Beijing University of Posts and Telecommunications, Beijing 100876, China

Corresponding authors: Weimin Wang (wangwm@bupt.edu.cn) and Yongle Wu (wuyongle138@gmail.com).

This work was supported by the National Natural Science Foundations of China under Grant 61701041, Grant 61272518, Grant 61327806, and Grant 61671478.

ABSTRACT The multi-probe anechoic chamber (MPAC) based method is a candidate to assess the performance of multiple input multiple output (MIMO) devices over the air. This paper investigates the core problem, channel emulation method (CEM), in MPAC setups. The CEM is utilized to map the desired channel onto the limited number of probes to synthesize the target channel environment within a certain test area. In addition, the channel in realistic propagation environment is a three-dimensional (3D) channel, which can achieve higher data transmission rate by containing both azimuth and elevation dimension. Hence, it is urgent to investigate the CEM for 3D channels in MPAC setups. In this paper, the implementation of a novel CEM for 3D channels is presented, which allocates the subpaths in a simple way and complements the drawbacks of prefaded synthesis method and spatial fading emulator. Furthermore, the impact of the target channel and probe configuration on the emulation accuracy in terms of temporal correlation function (TCF) and spatial correlation function (SCF) is discussed. Simulation results demonstrate that the emulation accuracy of TCF depends more on the motion direction of MIMO devices while that of SCF depends more on the probes distribution. Moreover, probes number decides the emulation accuracy first. If the same number of probes are applied, the coincidence of the probe configuration and the target channel determines the emulation accuracy.

INDEX TERMS Channel emulation method, multi-probe anechoic chamber, spatial correlation, temporal correlation.

I. INTRODUCTION

In order to meet the need of increasing data transmission rate, multiple input multiple output (MIMO) technique, which exploits the characteristic of the multipath channel without additional bandwidth or transmitting power [1], [2], is widely utilized in the radio communication system. However, with the increasing number of antennas adopted in MIMO devices, it is impossible to measure its performance with a conducted testing method. Over the air (OTA) testing for MIMO capable terminals emerges, which can assess the radio performance of MIMO device easily [3]. The multi-probe anechoic chamber (MPAC) based method is a candidate, which enables to reproduce the arbitrary propagation environment in a controllable and repeatable way in lab. The purpose of the MPAC method is to control the signals emitted from probes to reproduce propagation environment around the device under test (DUT) as accurately as possible [4], [5].

For MPAC method, on account of unknown of radiation pattern of DUT beforehand, it is an essential requirement to model the channel propagation environment and antennas separately [6]. The geometry-based stochastic channel models (GSCMs) are selected as the target channel models since they enable separation modeling of propagation channels and antennas at transmitter (Tx) and receiver (Rx) side, such as SCM, SCME, WINNER and so on [7]–[9]. For GSCMs, channel propagation environment realizations are generated with the geometrical principle by summing contributions of rays represented by amplitude, directions of departure and arrival and so on. Typically, a certain number of rays compose

The associate editor coordinating the review of this manuscript and approving it for publication was Huapeng Zhao.

a cluster which has a specific shaped power angular spectrum according to different propagation environments. The power angular spectrum is a probability density function obtained by statistical analysis through plenty of measurements for the realistic environment [7]. Three-dimensional (3D) channels can increase data transmission rate remarkably by containing both elevation and azimuth dimension. On the other hand, the realistic channel propagation environment is 3D. Hence, it is urgent to investigate the signals transmission in 3D channels. In addition, the related research on modeling 3D GSCMs is conducted in some organizations, such as 3rd Generation Partnership Project (3GPP), Nokia, and so on [10]–[13]. For the reproduced channel within a test area, it usually covers four domains of the channel, namely polarization, delay, time, and space, to evaluate its accuracy. The cross polarization power ratios (XPR) in polarization domain can be reproduced accurately by controlling the proportion of signals radiated from probes with orthogonal polarization. The power delay profile (PDP) in delay domain can be generated accurately by allocating the specific characteristic in the channel emulator [7]. Therefore, the temporal correlation function (TCF) in time domain and the spatial correlation function (SCF) in space domain are often utilized to assess the accuracy of the reproduced channel.

Channel emulation methods (CEMs) map the target channel onto the limited number of probes to synthesize the target channel, which differ in the signals radiated from probes. For example, each probe transmits a single sinusoid with a certain amplitude, doppler frequency and random initial phase for spatial fading emulator (SFE) [14]–[17] while each probe transmits sum of sinusoids for prefaded signal synthesis (PFS) [7], [9], [18]. In addition, different CEMs consider different aspects of the channel model as the target. For instance, plane wave synthesis (PWS) focuses on the synthesis of individual subpaths, in which the plane wave from an arbitrary direction observed within a test area is the target signal to generate [7]. Whereas, other CEMs emphasize the concept of cluster such as the PFS and SFE method. However, the SFE method is more sensitive to the number of probes especially when even number probes are utilized. The doppler spectra emitted from probes at different angular locations are the same for PFS, which is against with the reality [7]. The CEM proposed in [19] suggests that each probe transmits several sinusoids according to the probes location and target channel model, which is called the reference method in the following. The reference method can derive more accurate emulated channel than SFE under the same condition and complement the drawback of PFS. Its implementation for 3D channels is proposed in this paper. Similarly, in order to compare fairly with SFE, the number of subpaths equals the probes number. In this paper, temporal correlation function (TCF) and spatial correlation function (SCF) are utilized to assess the accuracy of the reproduced channel. The expressions of TCF and SCF using the reference method for 3D channels are given and the factors that affect the emulation accuracy of TCF and SCF are analyzed. Finally, the impact of the target channel and probe configuration on emulation accuracy is evaluated in terms of TCF and SCF in 3D MPAC setups.

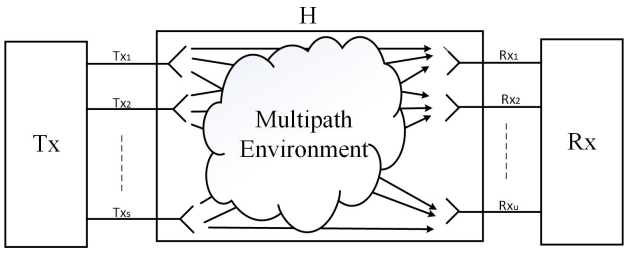

FIGURE 1. MIMO system block diagram [1].

The main contributions of this paper are listed in the following aspects:

- The implementation of the reference method for 3D channels is proposed to extend the 2D channels in [19] and the hardware requirement is given.
- The expressions of TCF and SCF of the emulated channel obtained by the reference method are derived and the analysis of the impact factors on the emulation accuracy of TCF and SCF is given.
- The emulation accuracy for 3D channels is investigated in terms of TCF and SCF under different conditions, such as target channel model, and probe configuration.

The paper is structured as below. In section II, we propose the implementation of the reference method for 3D channels, and derive the corresponding channel impulse responses applied in MPAC setups. In section III, we deduce the general expressions of TCF and SCF for the target channel and the emulated channel using the reference method and analyze the factors influencing the emulation accuracy of TCF and SCF. In Section IV, we present the emulation accuracy of the reference method under different conditions and give some analyses. Section V gives the conclusion of the paper.

II. CHANNEL EMULATION METHOD

Fig. 1 depicts an MIMO system with S antennas at the Tx side and U antennas at the Rx side. For GSCMs, the modeled propagation channel is only determined by the multipath environment expressed by channel transfer function H. On account of independent modeling of each cluster and polarization [6], only single cluster channel model and vertical polarization are considered for the sake of simplicity. The expression of the channel transfer function is written as [11], [20]

$$\begin{aligned} H_{u,s}(t,f) = \sum_{m=1}^{M} \sqrt{P_m} F_{tx,s} F_{rx,u} \exp\left(\mathrm{j}2\pi/\lambda \left(r_{tx,m}^T \cdot d_{tx,s}\right)\right) \\ \cdot \exp\left(\mathrm{j}2\pi/\lambda \left(r_{rx,m}^T \cdot d_{rx,u}\right)\right) \\ \times \exp\left(\mathrm{j}2\pi \vartheta_m t + \mathrm{j}\Phi_m\right) \exp\left(-\mathrm{j}2\pi f \tau_0\right) \end{aligned} \quad (1)$$

where M is the number of subpaths. P_m is the power of the mth subpath in the cluster. Φ_m is the random initial phase of the mth subpath, which follows a uniform distribution among

$[-\pi, \pi]$. ϑ_m is the doppler spectrum of the mth subpath. $d_{rx,u}$ and $d_{tx,s}$ are location vectors of the uth Rx and the sth Tx, respectively. λ is the wavelength of the carrier frequency. $r_{tx,m}$ and $r_{rx,m}$ are unit vectors for the departure angle and arrival angle of the mth subpath, respectively. f is the carrier frequency. τ_0 is the delay. $F_{tx,s}$ and $F_{rx,u}$ denote antenna patterns of the sth Tx and the uth Rx, respectively. The pattern is often assumed as omnidirectional for the Rx since its antenna pattern is typically not known beforehand [6].

The accuracy of the reproduced channel model at Rx side is investigated in this paper. Therefore, the characteristic at Tx side is fixed and expressed as a complex constant $c_{s,m}$, shown in (2). The reverse is also appropriate, only with the different channel model and antenna array.

$$c_{s,m} = \sqrt{P_m} F_{tx,s} \exp\left(\mathrm{j}2\pi/\lambda \left(r_{tx,m}^T \cdot d_{tx,s}\right)\right) \exp\left(-\mathrm{j}2\pi f \tau_0\right) \tag{2}$$

Substituting (2) into (1), the received signal of the uth Rx is expressed as

$$H_{u,s}(t) = \sum_{m=1}^{M} F_{rx,u} \exp\left(\mathrm{j}2\pi/\lambda \left(r_{rx,m}^T \cdot d_{rx,u}\right)\right) \times \exp\left(\mathrm{j}2\pi \vartheta_m t + \mathrm{j}\Phi_m\right) c_{s,m} \tag{3}$$

The purpose of the MPAC method is to reconstruct propagation channel $\hat{H}$ imitating H with the limited number of probes in MPAC setups. The signal received by the uth Rx within a test area for the CEM is written as [6]

$$\hat{H}_{u,s}(t) = \sum_{k=1}^{K} \hat{H}_{k,s}(t) \cdot \alpha_{k,u} F_{rx,u} \exp\left(\mathrm{j}2\pi/\lambda \left(r_k^T \cdot d_{rx,u}\right)\right) \tag{4}$$

where $\hat{H}_{k,s}(t)$ is the signal radiated from the kth probe, which is diverse for different CEMs. r_k is the unit vector for the location of the kth probe, expressed as $[\cos\theta_k \cos\varphi_k, \cos\theta_k \sin\varphi_k, \sin\theta_k]$ for 3D probe configuration. $d_{k,u}$ is the distance between the kth probe and the uth Rx. $\alpha_{k,u}$ denotes propagation coefficient from the kth probe to the uth Rx, which is expressed as [6]

$$\alpha_{k,u} = L\left(d_{k,u}\right) \times \exp\left(\mathrm{j}2\pi/\lambda d_{k,u}\right) \tag{5}$$

where $L(d_{k,u})$ is the path loss from the kth probe to the uth Rx, which is the same value for all sampling points within a test area when the radius of the probe ring is sufficiently large.

The hardware requirement for the reference method is depicted in Fig. 2. From Fig. 2, we can see that each probe connects with power divider, phase shifters, and attenuators, but not with base station emulator and channel emulator. Hence, the signals radiated from probes do not contain the characteristic of Tx side and temporal characteristic.

The angular locations of probes of 3D probe configuration in the upper figure are detailed in Table 1. Probes are distributed on the spherical surface with different elevation angles. Probes on the same elevation angle constitute a probe ring, on which probes uniformly distribute.

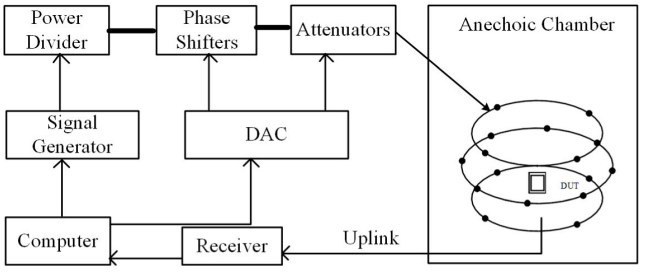

FIGURE 2. The diagram of the 3D MPAC setup for the reference method [3]. A 2D MPAC setup is only with the middle ring. The MPAC system consists of a signal generator, power divider, digital/analog converter (DAC), several phase shifters and attenuators, computer, multiple probe antennas located around DUT, and an anechoic chamber.

TABLE 1. Probe angular location details of setup A.

Setup	Detail	
	Total	Angular location
A	16	θ_1^k=-15° $\varphi_{1,j}^k$=-180°+j90° $j\in[1,\ldots,4]$
		θ_2^k=0° $\varphi_{2,j}^k$=-180°+j45° $j\in[1,\ldots,8]$
		θ_3^k=15° $\varphi_{3,j}^k$=-180°+j90° $j\in[1,\ldots,4]$

Compared with PFS and SFE to synthesize channels from the perspective of clusters, each probe transmits several subpaths according to channel models and angular locations of probes in the reference method. The signal radiated from the kth probe is calculated as

$$\hat{H}_k^{REF}(t) = \sum_{q=1}^{Q} \sqrt{g_{k,q}} \exp\left(\mathrm{j}2\pi \left(\vartheta_k + \Delta f_{k,q}\right) t + \mathrm{j}\Phi_{k,q}\right) \tag{6}$$

where $g_{k,q}$, $\Delta f_{k,q}$ and $\Phi_{k,q}$ denote the amplitude, frequency offset component and random initial phase, respectively, for the qth subpath allocated to the kth probe. ϑ_k is the doppler spectrum of the kth probe. Q is the number of subaths allocated to the kth probe. The total number of subpaths emitted from probes in the reference method equals the number of probes.

Taking the truncated Laplacian distribution for instance with 0° mean Azimuth angle Of Arrival (MAOA) and 35° Azimuth angle Spread of Arrival (ASA) for Power Azimuth Spectrum (PAS) and with 0° mean Zenith angle Of Arrival (MZOA) and 5° Zenith angle Spread of Arrival (ZSA) for power elevation spectrum (PES), the implementation of the reference method for 3D channels is depicted in Fig. 3.

For 3D implementation of the reference method, the elevation angle of the subpaths is determined by the elevation angle of probe rings to correspond to the SFE method. The implementation of subpaths on each probe ring is the same as that of 2D channels. That is, the subpaths on each probe ring are derived by a mixture of uniform power sampling method and uniform angular sampling method. In addition,

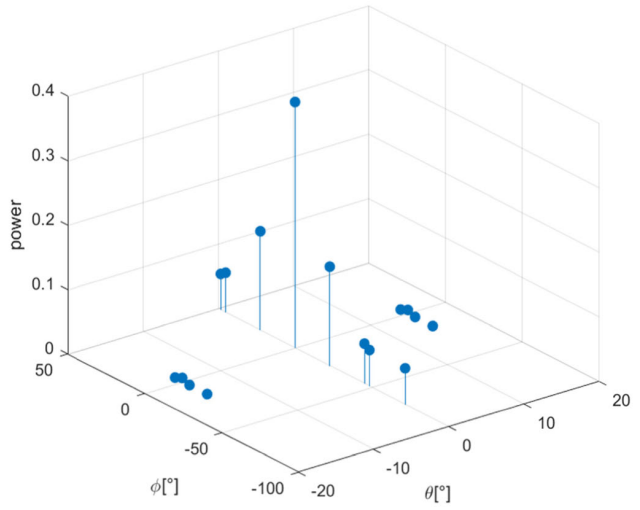

FIGURE 3. Implementation of the reference method for 3D channels. Φ axis and θ axis represent AOA and ZOA of the subpath, respectively. Power axis indicates the power value of the subpath for the reference method.

the subpaths number on each probe ring equals the probes number on the corresponding probe ring. Finally the subpaths are allocated onto the nearest probe to synthesize the channel.

The process of deriving the specific angle and power value of the subpath is presented in the following:

The elevation angles and PES of subpaths are calculated as

$$\begin{cases} \theta_i^m = \theta_i^k \\ p_e\left(\theta_i^m\right) = \dfrac{\sqrt{2}}{2\sigma_\theta} \exp\left(-\sqrt{2}\dfrac{\left|\theta_i^m - \bar{\theta}\right|}{\sigma_\theta}\right) \end{cases} \tag{7}$$

where $\theta_i^m$and θ_i^k denote the ith elevation angle in subpaths allocation and probe configuration, respectively. P_e is the power value in elevation dimension. $\bar{\theta}$ is MZOA and σ_θ is ZSA. Then we calculate the azimuth angle of the subpaths through the mixture of uniform angular sampling method and uniform power sampling method. For the uniform angular sampling method and uniform power sampling method, the initial number of subpaths on each probe rings is twice the number of probes on the same elevation angles. The azimuth angles and PAS of the subpaths for these two methods are calculated as

$$\begin{cases} \phi 1_{i,j}^m = -180^o + (j-1) \times \dfrac{360^o}{2J} \\ p1\left(\phi_{i,j}^m\right) = \dfrac{\sqrt{2}}{2\sigma_\phi} \exp\left(-\sqrt{2}\dfrac{\left|\phi_{i,j}^m - \bar{\phi}\right|}{\sigma_\phi}\right) \end{cases} \tag{8}$$

$$\begin{cases} \phi 2_{i,j}^m = \begin{cases} -\dfrac{\sigma_\phi}{\sqrt{2}} In(\dfrac{\sqrt{2}\sigma_\phi}{2J}) + \bar{\phi}, \phi_{i,j}^m > \bar{\phi} \\ \dfrac{\sigma_\phi}{\sqrt{2}} In(\dfrac{\sqrt{2}\sigma_\phi}{2J}) + \bar{\phi}, \phi_{i,j}^m < \bar{\phi} \end{cases} \\ p2\left(\phi_{i,j}^m\right) = \dfrac{1}{2J} \end{cases} \tag{9}$$

where $\phi 1_{i,j}^m$ and $\phi 2_{i,j}^m$ denote the azimuth angle of the jth subpath on the ith probe ring for uniform angular sampling method and uniform power sampling method, respectively. $p1$ and $p2$ denote the power value in azimuth dimension for uniform angular sampling method and uniform power sampling method, respectively. $\bar{\phi}$ is MAOA and σ_ϕ is ASA. J is the number of subpaths on each probe ring, which differs for different probes rings, such as 4, 8, 4 subpaths for probe ring 1, 2, and 3 in setup A, respectively. Then we choose part of subpaths to form the new collection representing channel environment. The selection method is

$$\text{If } p1\left(\phi_{i,j}^m\right) > 1/(2J), \begin{cases} \phi_{i,j}^m = \phi 1_{i,j}^m \\ p_a\left(\phi_{i,j}^m\right) = p1\left(\phi_{i,j}^m\right) \end{cases}$$

$$\text{else} \begin{cases} \phi_{i,j}^m = \phi 2_{i,j}^m \\ p_a\left(\phi_{i,j}^m\right) = p2\left(\phi_{i,j}^m\right) \end{cases}$$

where $\phi_{i,j}^m$ denotes the azimuth angle of the jth subpath on the ith probe ring. p_a is the corresponding power in azimuth dimension. If the number of the subpaths in the new collection is larger than the number of probes, the subpaths at the large offset angle from MAOA will be removed. If the number of subpaths in the new collection is less than the number of probes, the subpaths derived by uniform power sampling method near MAOA is added to the collection. Finally, we derive the ultimate collection, in which the number of subpaths equals the number of probes. And the power value of the subpath is the product of P_e and P_a.

III. FIGURE OF MERIT

The emulation accuracies of TCF and SCF for the emulated channel are selected as the criteria to reflect the accuracy of the emulated channel imitating the target channel in MPAC setups. Because PDP and XPR can be reconstructed accurately by setting appropriate power and polarization for each cluster and polarization dimension, they are omitted in this paper.

A. TEMPORAL CORRELATION FUNCTION

TCF can be used as the criterion to evaluate how well the temporal characteristic of the emulated channel approximates that of the target one. It reflects the similarity of the received signals by the Rx antenna at different times. According to the definition of the correlation, the expression of TCF is written as

$$\rho_\tau = \frac{1}{\beta_\tau} \mathrm{E}\left\{H_u\left(t+\tau\right) H_u\left(t\right)^*\right\} \tag{10}$$

where β_τ is the normalization factor to force $\rho_\tau = 1$ when $\tau = 0$. Substituting (1) into (10), the expression of TCF for the target channel is written as

$$\rho_\tau^{tar} = \frac{1}{\beta_\tau^{tar}} \sum_{m=1}^{M} P_m \exp\left(\mathrm{j}2\pi\vartheta_m\tau\right) \tag{11}$$

Similarly, the emulated TCF for the reference method can be deduced by the corresponding expression, which is written

as

$$\hat{\rho}_{\tau}^{REF} = \frac{1}{\hat{\beta}_{\tau}^{REF}} \sum_{k=1}^{K} \sum_{q=1}^{Q} g_{k,q} \exp\left(\mathrm{j}2\pi \left(\vartheta_k + \Delta f_{k,q}\right)\tau\right) \quad (12)$$

where β_{τ}^{tar}, $\hat{\beta}_{\tau}^{REF}$ are the normalization factors for the target TCF and the emulated TCF obtained by the reference method, respectively.

From the expressions of TCF, it can be inferred that the target TCF is determined by the target channel and the velocity of DUT, while the emulated TCF is also determined by probe configuration and probe weights. The absolute value of the deviation between the target TCF and the emulated TCF is selected as the criterion to evaluate emulation accuracy of the emulated TCF, which is calculated as $\left|\left|\rho_{\tau}^{tar}\right| - \left|\hat{\rho}_{\tau}^{REF}\right|\right|$. Hence, the performance of the emulated TCF depends on the velocity of DUT, probe configuration, and probe weights which are determined by probe configuration and target channel.

B. SPATIAL CORRELATION FUNCTION

SCF is an appropriate criterion of the spatial dimension, which is the similarity of the received signals by different Rx antennas within a test area. The expression of SCF is written as [9]

$$\rho_{u_1,u_2} = \frac{1}{\beta_0} E\left\{H_{u_1}(t) H_{u_2}(t)^*\right\} \quad (13)$$

where β_0 is the normalization factor to force $\rho_{u_1,u_2} = 1$ when $u_1 = u_2$. Substituting (1) into (13), the expression of the SCF for the target channel can be written as

$$\rho_{u_1,u_2}^{tar} = \frac{1}{\beta_0^{tar}} \sum_{m=1}^{M} P_m \exp\left(\mathrm{j}2\pi/\lambda r_{rx,m}^{T} \cdot \left(d_{rx,u_1} - d_{rx,u_2}\right)\right) \quad (14)$$

The expressions of SCF for the emulated channel by the reference method can be written as

$$\hat{\rho}_{u_1,u_2}^{REF} = \frac{1}{\hat{\beta}_0^{REF}} \sum_{k=1}^{K} \exp\left(\mathrm{j}2\pi/\lambda r_{k}^{T} \cdot \left(d_{rx,u_1} - d_{rx,u_2}\right)\right) \cdot \sum_{q=1}^{Q} g_{k,q} \quad (15)$$

where β_0^{tar}, $\hat{\beta}_0^{REF}$ are the normalization factors for the target SCF and the emulated SCF obtained by the reference method, respectively.

From the expressions of SCF, we can infer that the target SCF is determined by the target channel and the location of Rx antennas pair, while the emulated SCF is also determined by the probe configuration and probe weights. The root mean square (rms) of the deviation between the emulated SCF and the target SCF is selected to evaluate the emulation accuracy in spatial dimension, which is calculated as

$$\sigma_{rms} = \sqrt{\frac{1}{SP} \sum_{sp=1}^{SP} \left|\rho_{u_1,u_2}^{tar} - \hat{\rho}_{u_1,u_2}^{REF}\right|^2} \quad (16)$$

where SP is the number of Rx antennas pair to sample the test area. Hence, the performance of the emulated SCF depends on the probe configuration, the location of Rx antennas pair, and probe weights which are determined by target channel and probe configuration.

IV. SIMULATION ANALYSIS

The results of how well the emulated channel matches the target channel in terms of TCF and SCF at Rx side are presented for 3D channels in this section. Moreover, the DUT motion direction is 0° in azimuth dimension and 0° in elevation dimension. Rx antennas pairs are sampled on 3D spherical surface. In this section, the impact of target channel, and probe configuration on the emulation accuracy is investigated.

A. IMPACT OF TARGET CHANNEL ON EMULATION ACCURACY

In this section, we emulate different 3D spherical power spectra (SPS), which can be decomposed into PAS and PES, in 3D MPAC setups. PAS and PES are utilized to describe the channel environment in azimuth and elevation dimension, respectively. In this paper, the truncated Laplacian distributions with different arrival angles and angle spreads are selected as the target SPS.

1) IMPACT OF MAOA AND ASA AT 0° ZSA AND 0° MZOA

When ZSA and MZOA are both set as 0°, the impact of MAOA and ASA on the emulation accuracy is presented in Fig. 4. It approximates a two-dimensional (2D) channel.

From Fig. 4, we can observe that the emulation accuracy is relative with MAOA especially when ASA is small. For the simulation results of TCF, when the target channel impinges from the direction of DUT motion direction or in the same line, the emulation accuracy gets the best results while it gets poor results for MAOA perpendicular to DUT motion direction, such as ±90° MAOA. However, the emulation accuracy of SCF presents different results. When MAOA is between two probes, it presents the worst results. Furthermore, when ASA is large, the target channel approaches a uniform distribution in horizontal plane. Hence, the emulation accuracy is irrelative with the MAOA at this case.

2) IMPACT OF MZOA AND ZSA AT 0° ASA AND 0° MAOA

The impact of MZOA and ZSA at 0° ASA and 0° MAOA on the emulation accuracy of TCF and SCF is depicted in Fig. 5.

The deviation increases when the absolute value of MZOA increases. Compared to MZOA, ZSA less affects the emulation accuracy. In addition, the difference between the emulation accuracy of TCF and SCF occurs at small ZSAs.

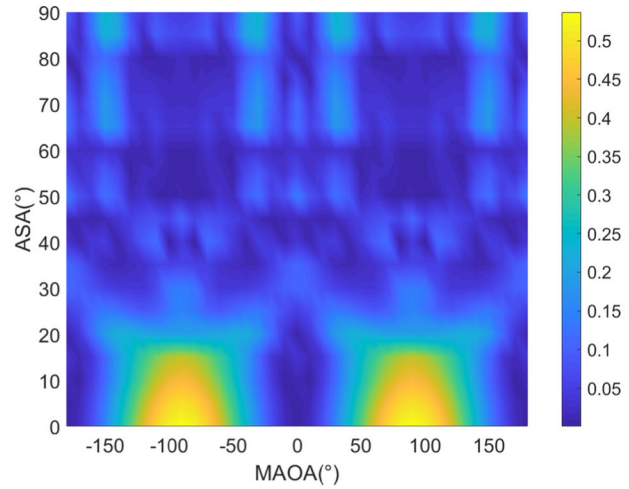

(a) TC

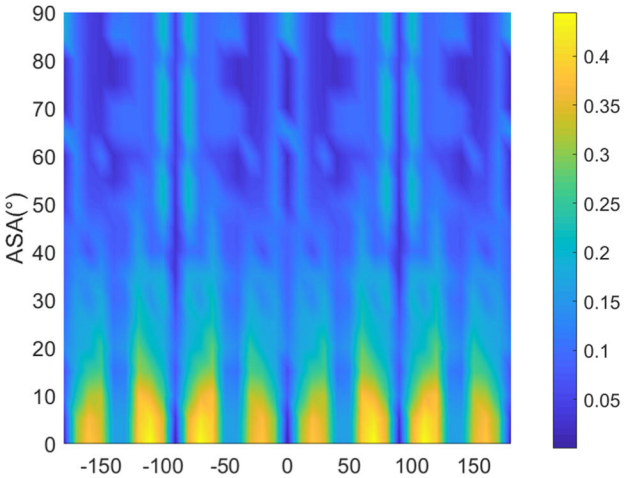

(b) SCF

FIGURE 4. Effect of MAOA and ASA on the emulation accuracy of TCF and SCF.

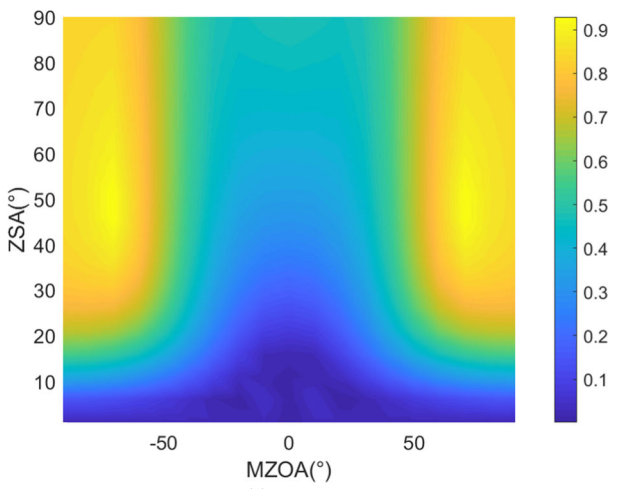

(a) TCF

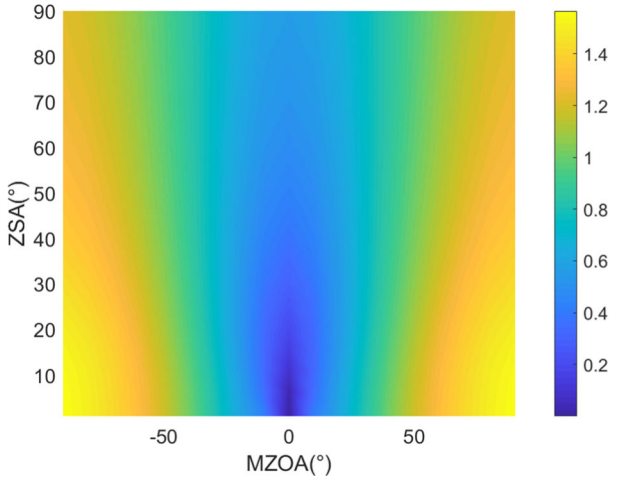

(b) SCF

FIGURE 5. Effect of ZSA and MZOA on the emulation accuracy of TCF and SCF.

When ZSA is small, the emulation accuracy of TCF is not affected by the MZOA and it presents better results. Whereas, the emulation accuracy of SCF is affected by MZOA and it presents worse results at large aboslute value of MZOA. The opposite results for the simulation results of TCF and SCF can be explained by the following two reasons. For TCF, the selection of DUT motion direction, the normalization of SPS and elevation angle distribution of probes together cause the result that the emulated TCF almost equals the target TCF when ZSA is small. That is the absolute value of the TCF is close to 1 for the above two situations. Hence, the emulation accuracy of TCF performs better at small ZSA. However, for the simulation of SCF, no probe locates at two poles, which causes inaccurate results for larger MZOA at small ZSA. Furthermore, with the increase of ZSA, the emulation accuracy is improved for the simulation results of SCF. That is, compared to small ZSA, the same deviation value occurs at larger absoulte value of MZOA when ZSA is large.

3) IMPACT OF MZOA AND MAOA AT 35° ASA AND 5° ZSA

The impact of MZOA and MAOA at 35° ASA and 5° ZSA on the emulation accuracy of TCF and SCF is demonstrated in Fig. 6.

For the simulation of TCF, we can derive that when the absolute value of MZOA is small, the emulation accuracy performs worst when MAOA is perpendicular to DUT motion direction, which is in accord with the results in Section IV-A-1). When MZOA is around ±90°, which is also perpendicular to DUT motion direction, the maximum appears at other MAOAs rather than ±90°. For the simulation of SCF, the effect of MAOA on the emulation accuracy of SCF weakens. The emulation accuracy deteriorates at 0°, ±90° and ±180° MAOA when the absolute value of MZOA is large. In addition, the deviation between the target SCF and the emulated SCF increases with increasing MZOA. That is because no probe locates at two poles.

4) IMPACT OF ZSA AND ASA AT 0° MAOA AND 0° MZOA

The impact of ZSA and ASA at 0° MAOA and 0° MZOA on the emulation accuracy of TCF and SCF is demonstrated

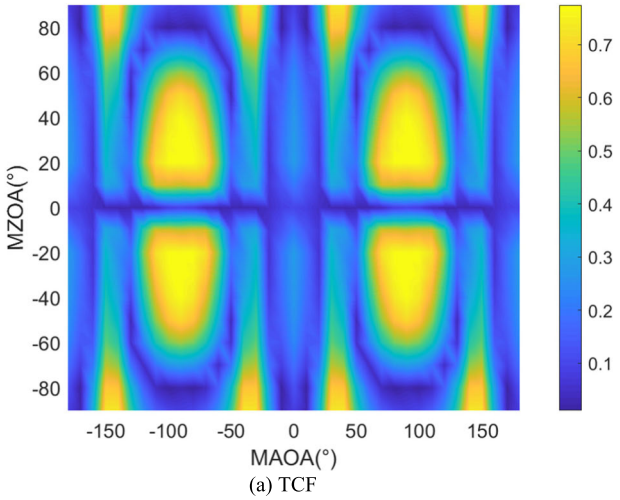

FIGURE 6. Effect of MZOA and MAOA on the emulation accuracy of TCF and SCF.

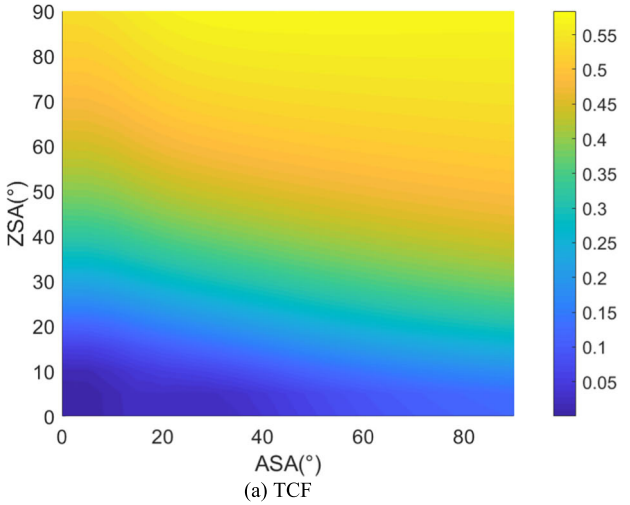

FIGURE 7. Effect of ZSA and ASA on the emulation accuracy of TCF and SCF.

in Fig. 7. From Fig. 7, we can observe that the deviation increases with increasing ZSA and ASA. That is because the target channel approaches a uniform distribution with increasing ASA and ZSA but only limited number of probes are utilized to synthesize the target continuous channel. Furthermore, the variation tendency is more obvious with varying ZSA.

B. IMPACT OF PROBE CONFIGURATION ON EMULATION ACCURACY

In this section, we discuss the effect of probe configuration on the emulation accuracy in 3D MPAC setups.

1) IMPACT OF ELEVATION ANGLE OF PROBE RING

The diagram of the 3D probe configuration utilized in this section is shown in Fig. 8. The angular location of probes and probes number are detailed in Table 2. According to the elevation angle of probe configuration, MZOA of the target channel is specified as 0°, 15° and 30°. Besides, MAOA, ASA, and ZSA are set as 0°, 35°, and 15°, respectively.

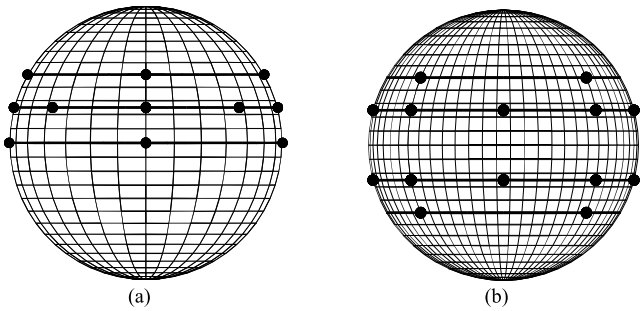

FIGURE 8. 3D probe configuration (a) setup B (b) setup C.

Fig. 9 plots the simulation results of TCF and SCF when probe configurations with different probes distributions in elevation dimension are utilized in 3D MPAC setups. From Fig. 9, we can observe that setup C presents the best results in general situations, which is benefited from the richness of its probes location. Furthermore, we can see that when MZOA is 0°, setup B presents the worst result while setup

TABLE 2. Probe angular location details of setups B and C.

Setup	Detail	
	Total	Angular location
B	16	θ_1=0° φ_{1j}=-180°+j90° $j\in[1,\ldots,4]$
		θ_2=15° φ_{2j}=-180°+j45° $j\in[1,\ldots,8]$
		θ_3=30° φ_{3j}=-180°+j90° $j\in[1,\ldots,4]$
C	24	θ_1=-30° φ_{1j}=-180°+j90° $j\in[1,\ldots,4]$
		θ_2=-15° φ_{2j}=-180°+j45° $j\in[1,\ldots,8]$
		θ_3=15° φ_{3j}=-180°+j45° $j\in[1,\ldots,8]$
		θ_4=30° φ_{4j}=-180°+j90° $j\in[1,\ldots,4]$

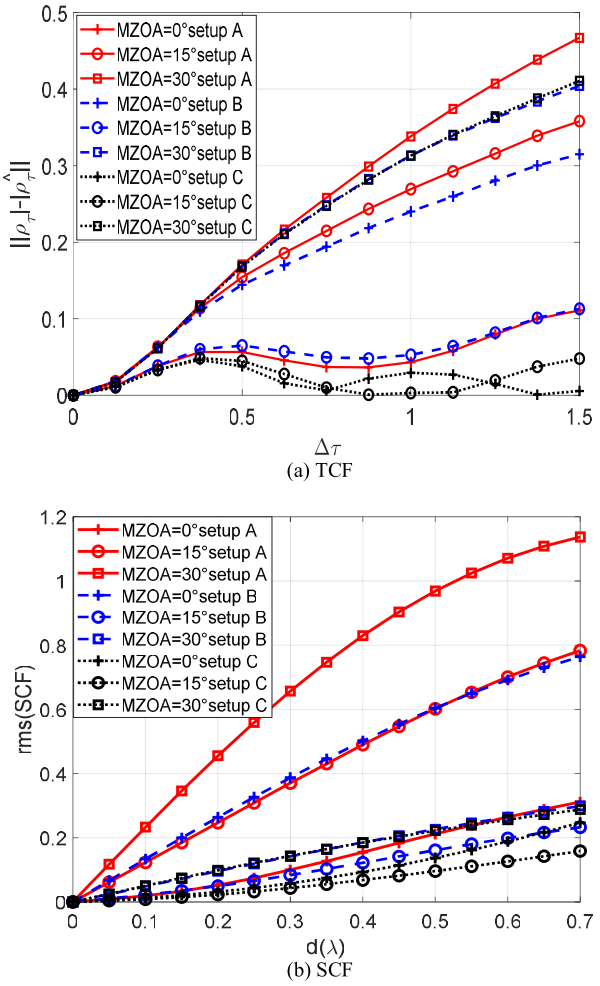

FIGURE 9. Effect of probe configuration on the emulation accuracy of TCF and SCF.

A presents the worst results when MZOA is 15° and 30°. For the simulation of TCF, Fig. 9(a) presents that setup B and setup C get the same results when MZOA is 30°. At the same time, the emulation accuracy of setup A when MZOA is 0° is roughly the same as that of setup B when MZOA is 15°. That is because the same probe configuration is set at the corresponding elevation angle. From Fig. 9(b), we can observe that the simulation result of SCF is roughly the same as that of TCF. The difference between the simulation results

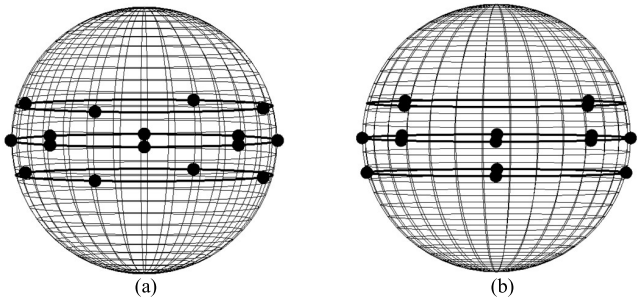

FIGURE 10. 3D probe configuration (a) setup D (b) setup E.

TABLE 3. Probe angular location details of setups D and E.

Setup	Detail	
	Total	Angular location
D	16	θ_1=-15° φ_{1j}=-180°+j90° $j\in[1,\ldots,4]$
		θ_2=0° φ_{2j}=-180°+22.5°+j45° $j\in[1,\ldots,8]$
		θ_3=15° φ_{3j}=-180°+j90° $j\in[1,\ldots,4]$
E	16	θ_1=-15° φ_{1j}=-180°+45°+j90° $j\in[1,\ldots,4]$
		θ_2=0° φ_{2j}=-180°+j45° $j\in[1,\ldots,8]$
		θ_3=15° φ_{3j}=-180°+j90° $j\in[1,\ldots,4]$

of TCF and SCF lies in the following two points: 1) for SCF, the emulation accuracy of setup A when MZOA is 15° equals that of setup B when MZOA is 0°. Whereas, for TCF, the emulation accuracy of setup A when MZOA is 0° equals that of setup B when MZOA is 15°; 2) when MZOA is 30°, setup B performs better than 0° MZOA for SCF. Hence, probes number determines the emulation accuracy at first. The emulation accuracy depends on the relationship between the target channel and probe configuration when the same number of probes are utilized.

2) IMPACT OF AZIMUTH ANGLE OF PROBE RING

By rotating the azimuth angle of each probe ring, we derive the 3D probe configuration utilized in this section shown in Fig. 10. The angular locations of probes and probes number are detailed in Table 3. According to the azimuth angle of probe configuration, MAOA of the target channel is specified as 0°, 22.5° and 45°. Also, MZOA, ASA, and ZSA are set as 0°, 5°, and 15°, respectively.

Fig. 11 presents the impact of probe configuration with different azimuth angles on the emulation accuracy. For the simulation of TCF, the emulation accuracy is diverse for varying MAOA. That is because with the increase of MAOA, the angle between the motion direction and MAOA increases. Hence, deviation increases until MAOA is perpendicular to the motion direction. Whereas, the emulation accuracy is irrelative with the probe configuration with different azimuth angles. For the simulation of SCF, from Fig. 11(b), we can observe that setup A performs best when MAOA is 0°, and it performs worst when MAOA is 22.5°. For setup D, the best result occurs at 22.5° MAOA due to a probe on probe ring 1 locating at this azimuth angle. For setup E, when MAOA is 22.5°, the emulation accuracy gets the worst result and the same emulation accuracy occurs at 0° and 45° MAOA.

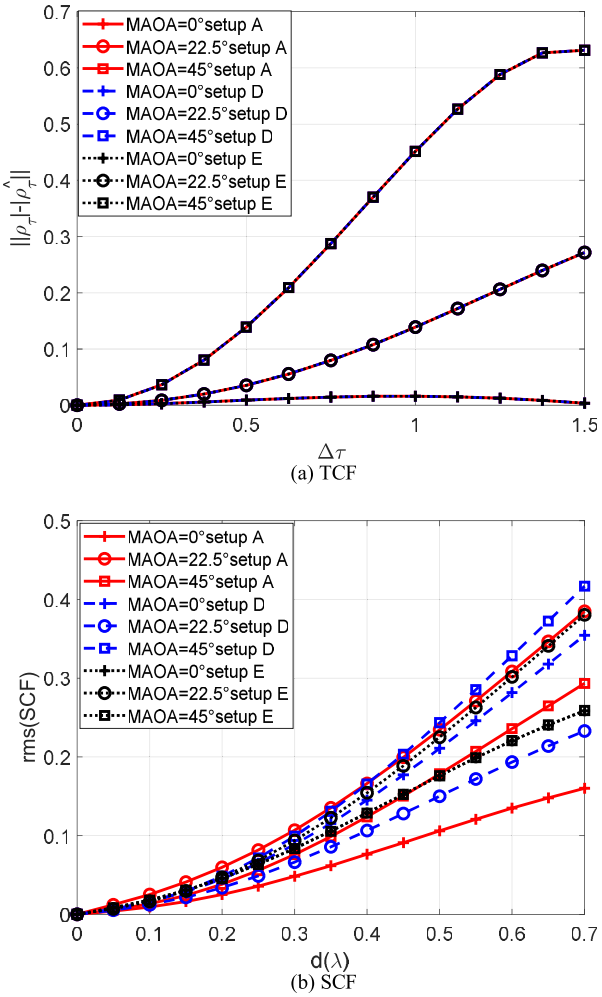

FIGURE 11. Effect of probe configuration on the emulation accuracy of TCF and SCF.

By comparing the three cases in which one probe locates at the same azimuth angle, setup D when MAOA is 22.5° performs better than setup A when MAOA is 45°. At the same time, it performs worse than setup A when MAOA is 0°. By comparing the two cases in which two probes locate at the same azimuth angle, when MAOA is 0°, setup E performs better than setup D. Setup A when MAOA is 0° gets the best result due to three probes locating at the same azimuth angle.

V. CONCLUSION

In this paper, we propose the implementation of the reference method to emulate 3D channels. Then we investigate the impact of the target channel and probe configuration on the emulation accuracy in terms of TCF and SCF under different conditions.

The investigation on the target channel is divided into four parts, namely MAOA and ASA, MZOA and ZSA, MZOA and MAOA, plus ZSA and ASA. When MAOA is perpendicular to DUT motion direction, the emulation accuracy of TCF gets the worst results. However, the emulation accuracy of SCF is determined by the probe configuration. That is, when the target channel impinges from the direction between two probes, the emulation accuracy gets the worst results. Compared to ZSA, the emulation accuracy is more effected by MZOA. With the increase of ZSA and ASA, the deviation decreases especially for ZSA.

The research on the probe configuration is divided into two aspects, namely elevation angle and azimuth angle of probes. The emulation accuracy is determined by probes number first. When the same number of probes are utilized to synthesize the channel, probe configuration which coincides with the target channel obtains more precise results.

REFERENCES

[1] M. A. Jensen and J. W. Wallace, "A review of antennas and propagation for MIMO wireless communications," *IEEE Trans. Antennas Propag.*, vol. 52, no. 11, pp. 2810–2824, Nov. 2004.

[2] J. G. Andrews, S. Buzzi, W. Choi, S. V. Hanly, A. Lozano, A. C. K. Soong, and J. C. Zhang, "What will 5G be?" *IEEE J. Sel. Areas Commun.*, vol. 32, no. 6, pp. 1065–1082, Jun. 2014.

[3] M. Rumney, R. Pirkl, M. H. Landmann, and D. A. Sanchez-Hernandez, "MIMO over-the-air research, development, and testing," *Int. J. Antennas Propag.*, vol. 2012, May 2012, Art. no. 467695.

[4] W. Fan, P. Kyösti, Y. Ji, L. Hentilä, X. Chen, and G. F. Pedersen, "Experimental evaluation of user influence on test zone size in multi-probe anechoic chamber setups," *IEEE Access*, vol. 5, pp. 18545–18556, 2017.

[5] W. Wang, H. Gao, Y. Wu, and Y. Liu, "Impact of probe configurations on maximum of test volume size in 3D MIMO OTA testing," *Wireless Commun. Mobile Comput.*, vol. 2017, Dec. 2017, Art. no. 2716149.

[6] W. Fan, P. Kyösti, J. Ø. Nielsen, and G. F. Pedersen, "Wideband MIMO channel capacity analysis in multiprobe anechoic chamber setups," *IEEE Trans. Veh. Technol.*, vol. 65, no. 5, pp. 2861–2871, May 2016.

[7] P. Kyösti, T. Jämsä, and J.-P. Nuutinen, "Channel modelling for multi-probe over-the-air MIMO testing," *Int. J. Antennas Propag.*, vol. 2012, Mar. 2012, Art. no. 615954.

[8] W. Fan, X. Carreno, P. Kyösti, J. O. Nielsen, and G. F. Pedersen, "Over-the-air testing of MIMO-capable terminals: Evaluation of multiple-antenna systems in realistic multipath propagation environments using an OTA method," *IEEE Veh. Technol. Mag.*, vol. 10, no. 2, pp. 38–46, Jun. 2015.

[9] Y. Ji, W. Fan, G. F. Pedersen, and X. Wu, "On channel emulation methods in multiprobe anechoic chamber setups for over-the-air testing," *IEEE Trans. Veh. Technol.*, vol. 67, no. 8, pp. 6740–6751, Aug. 2018.

[10] *Study on 3D Channel Model for LTE (Release 12)*, document TR 36.873, V12.7.0, 3rd Generation Partnership Project (3GPP), Dec. 2017.

[11] J. Zhang, C. Pan, F. Pei, G. Liu, and X. Cheng, "Three-dimensional fading channel models: A survey of elevation angle research," *IEEE Commun. Mag.*, vol. 52, no. 6, pp. 218–226, Jun. 2014.

[12] B. Mondal, T. A. Thomas, E. Visotsky, F. W. Vook, A. Ghosh, Y.-H. Nam, Y. Li, J. Zhang, M. Zhang, Q. Luo, Y. Kakishima, and K. Kitao, "3D channel model in 3GPP," *IEEE Commun. Mag.*, vol. 53, no. 3, pp. 16–23, Mar. 2015.

[13] *Spatial Channel Model for Multiple Input Multiple Output (MIMO) Simulations (Release 13)*, document 3GPP TR 25.996, V13.1.0, Dec. 2016.

[14] H. Arai, "Field simulator for Rayleigh/Rician fading reproduction," in *IEEE Antennas Propag. Soc. Int. Symp. Dig.*, Baltimore, MD, USA, Jul. 1996, pp. 1218–1221.

[15] H. Iwai, A. Yamamoto, T. Sakata, K. Ogawa, K. Sakaguchi, and K. Araki, "Spatial fading emulator for handset antennas," in *Proc. IEEE Antennas Propag. Society Int. Symp.*, Washington, DC, USA, Jul. 2005, pp. 218–221.

[16] H. Iwai, K. Sakaguchi, T. Sakata, and A. Yamamoto, "Performance evaluation of spatial correlation characteristics for handset antennas using spatial fading emulator based on Clarke's model," *IEICE Trans.*, vol. E93-B, no. 10, pp. 2514–2522, 2010.

[17] K. Honda and K. Li, "Three-dimensional MIMO-OTA calibration to achieve the Gaussian angular power spectra in elevation," *IEICE Commun. Express*, vol. 5, no. 10, pp. 394–400, 2016.

[18] A. Khatun, V.-M. Kolmonen, V. Hovinen, D. Parveg, M. Berg, K. Haneda, K. I. Nikoskinen, and E. T. Salonen, "Experimental verification of a plane-wave field synthesis technique for MIMO OTA antenna testing," *IEEE Trans. Antennas Propag.*, vol. 64, no. 7, pp. 3141–3150, Jul. 2016.

[19] R. Wang, Y. Ding, W. Wang, L. Chen, Y. Wu, and Y. Liu, "A novel channel emulation method in multi-probe anechoic chamber setups," in *Proc. 37th Int. Conf. Consum. Electron. (ICCE)*, Las Vegas, NV, USA, Jan. 2019, pp. 1–5.

[20] *Measurement of Radiated Performance for Multiple Input Multiple Output (MIMO) and Multi-Antenna Reception for High Speed Packet Access (HSPA) and LTE Terminals (Release 15)*, document TR 37.976, V15.0.0, 3rd Generation Partnership Project (3GPP), Sep. 2018.

WEIMIN WANG received the B.S. degree in communication engineering, the M.S. and Ph. D. degrees in electronic engineering from the Beijing University of Posts and Telecommunications (BUPT), Beijing, China, in 1999, 2004, and 2014, respectively. In 2014, she joined BUPT, where she is currently an Associate Professor with the School of Electronic Engineering. Her research interests include electromagnetic field and MIMO OTA measurement.

RURU WANG received the B.S. degree in electronic information science and technology from the University of Electronic Science and Technology of China (UESTC), Chengdu, China, in 2016, and the M.S. degree in electronic science and technology from the Beijing University of Posts and Telecommunications (BUPT), Beijing, China, in 2019. She is currently engaged in robotic process automation and artificial intelligence in aibank, Beijing.

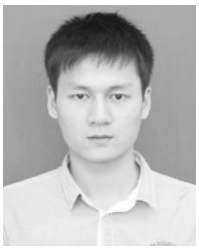

HUAQIANG GAO received the B.E. degree in electronic and information engineering from the Harbin University of Science and Technology, and the B.A. degree in business english from Heilongjiang University, Harbin, China, in 2016. He is currently pursuing the Ph.D. degree in electronic science and technology with the Beijing University of Posts and Telecommunications, Beijing, China. Since 2018, he has been a Research Intern with the Antennas, Propagation and Millimeter-wave Systems Section, Aalborg University. His research interest includes the air testing of wireless devices.

YONGLE WU received the B.Eng. degree in communication engineering and the Ph.D. degree in electronic engineering from the Beijing University of Posts and Telecommunications (BUPT), Beijing, China, in 2006 and 2011, respectively. From April 2010 to October 2010, he was a Research Assistant with the City University of Hong Kong (CityU), Kowloon, Hong Kong. In 2011, he joined the BUPT, where he is currently a Full Professor with the School of Electronic Engineering. His research interests include microwave components and wireless systems design.